Long-Path THz-TDS Atmospheric Measurements Between Buildings

Eom-Bae Moon, Tae-In Jeon, and Daniel R. Grischkowsky, *Fellow, IEEE*

***Abstract*—We have measured THz pulse propagation through a 186 m distance for which the THz pulses propagated in the atmosphere between two buildings separated by 79.3 m, with different relative humidity (RH) and weather conditions such as clouds, rain, and snow. The THz pulses propagated through rain falling at 3.5 mm/h and snow falling at 2 cm/h equivalent to 2.0 mm/h rainfall. For calm weather, the transmitted THz pulseshapes and relative transit times were measured to a precision of 0.1 ps. These broadband measurements demonstrate the potential of line-of-sight THz communications, THz sensing, and THz imaging through fog and smoke.**

***Index Terms*—Atmospheric absorption, Terahertz (THz) spectroscopy, THz communications, THz-TDS.**

I. Introduction

THE understanding of atmospheric transparency in the THz frequency range is important to many applications such as ground- and space-based communications and remote sensing [1]–[3]. The water content of the atmosphere is an important factor in determining the THz transmission. In general, the amount of water vapor in the atmosphere and the THz transmission have an inverse relationship. Many scientists have measured the relationship with different relative humidity, altitudes, and locations [4]–[8].

Emery *et al.* have made long-path field measurements from 0.15 to 0.51 THz, using an FTIR spectrometer with 6 GHz resolution, of the atmospheric amplitude transmission spectrum for horizontal beam propagation 2 m above ground level in a sea level atmosphere for distances of up to 500 m [6]. They measured transmission as a function of temperature (270–290 K), and water vapor density (WVD) from 4 to 11 g/m^3. Their results for water vapor were compared to monomer theory over the frequency range of 150–450 GHz, and showed higher absorption, which was attributed to the continuum absorption due to water dimers. They also measured the attenuation for a long-path passage through fog. Recently, D. Grischkowsky's group has measured within a building the long-path atmospheric complex transmission spectrum (both amplitude and phase) from 0.1 up to 2.0 THz, using a THz time-domain spectroscopy (THz-TDS) system with 6.1 GHz resolution [8]–[11]. They measured transmission through a 137 m path within a humidity controlled sample chamber, as a function of relative humidity from 4% to 51% at 21 °C. More recently, they measured broadband THz pulse propagation through a dense artificial fog for a 137 m long THz beam path within the sample chamber [12]. Although these studies measured the attenuation spectra of water vapor under different sample chamber conditions, it was not possible to duplicate the atmospheric weather conditions, having winds, turbulence and inhomogeneity in temperature and density.

Long path THz-TDS studies under atmospheric weather conditions can provide information for the important THz atmospheric applications of communications, sensing, imaging through fog and smoke [12], and measuring time dependent changes in distances up to hundreds of meters to a precision of 30 microns.

The results presented here are to be considered as a "proof of concept" of the potential of outdoor long-path THz-TDS to characterize the absorption and dispersion of rain and snow in the atmosphere from 100 to 1000 GHz. An important feature is that the measured long-path THz pulses have a signal-to-noise ratio (SNR) better than 100 (peak-to-peak of the THz pulse)/(peak-to-peak of the noise fluctuations in front of the pulse). We describe the first outside, long-path THz-TDS measurements between buildings [13]. These attenuation measurements were made under various weather conditions, including rain and snow. The THz beam propagates between two buildings separated by 79.3 m, for which the total round trip path between the transmitter and receiver is 186 m.

The long-term objective of these THz-TDS measurements is to characterize (to an accuracy of $\pm 1\%$) the outside atmosphere from 50 GHz to 1 THz with respect to attenuation, scattering and dispersion under various weather conditions, and other conditions, such as fire, smoke and gas plumes.

II. Experimental Setup

For the THz-TDS technique the temporal electric field amplitude of two electromagnetic THz pulses are measured; the reference input pulse and the transmitted output (sample) pulse,

Manuscript received February 04, 2015; revised April 02, 2015; accepted May 26, 2015. Date of publication July 28, 2015; date of current version August 31, 2015. This work was supported in part by a National Research Foundation of Korea (NRF) grant funded by the Korea government (MSIP) under 2013R1A1A2A10004669, and by the World Class Institute (WCI) Program of the National Research Foundation of Korea (NRF) funded by the Ministry of Science, ICT and Future Planning under NRF Grant WCI 2011-001. *(Corresponding author: Tae-In Jeon.)*

E.-B. Moon is with the Division of Electrical and Electronics Engineering, Korea Maritime and Ocean University, Busan, 606-791, and also with the Center for Quantum-Beam-based Radiation Research, Korea Atomic Energy Research Institute, Daejeon, 305-353, South Korea (e-mail: moonintro@gmail.com).

T.-I. Jeon is with the Division of Electrical and Electronics Engineering, Korea Maritime and Ocean University, Busan, 606-791, South Korea (e-mail: jeon@kmou.ac.kr).

D. R. Grischkowsky is with the School of Electrical and Computer Engineering, Oklahoma State University, Stillwater, OK 74078 USA (e-mail: daniel.grischkowsky@okstate.edu).

Color versions of one or more of the figures in this paper are available online at http://ieeexplore.ieee.org.

Digital Object Identifier 10.1109/TTHZ.2015.2443491

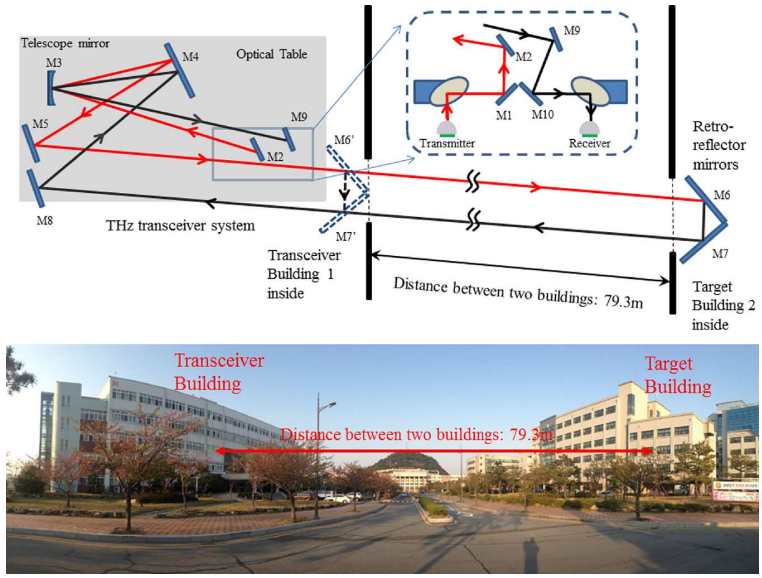

Fig. 1. (top) Schematic of long-path setup. Red line is the outgoing THz beam. Black line is the reflected incoming beam. (bottom) Photograph of transceiver building and target building.

which has changed shape due to passage through the sample under study. Through Fourier analyses of the input and output pulses the frequency-dependent absorption and dispersion of the sample can be obtained.

A schematic diagram of the long-path setup is shown in Fig. 1 [13]. All optical mirrors and the standard THz-TDS system are on an optical table on the third floor of the Transceiver Building 1, except for the two-dimensional retro-reflector mirrors (M6 and M7) which are installed with a stable heavy mounting on the third floor of the Target Building 2. The two buildings are 79.3 m away from each other for the line of sight THz beam paths. The THz beams propagate 142 cm above the third floor level of the five floor Buildings 1 and 2. The ground level of the buildings is located about 3 m above the mean sea level, and the THz beams travel 9.5 m above the ground, between the buildings. For both buildings the glass windows in the THz beam-path are replaced with a 20 μm thin plastic film, to minimize absorption loss and reflections and to protect the THz transceiver system and mirrors from the outside environment. Because the film thickness is much smaller than the THz wavelength, the transmission is increased and the reflection is reduced to be much better than for glass, which absorbs THz radiation. For 0.3 THz with 1 mm wavelength the amplitude transmission is 99.4% and the corresponding amplitude reflection is 11%.

The THz pulses are opto-electronically generated and detected on photoconductive semi-insulating GaAs and low temperature grown GaAs chips, respectively. A Spectra-Physics Mai-Tai, 790 nm, 50 fs pulse, Ti:Sapphire Mode-locked laser beam with a pulse repetition rate of 84.01 MHz was divided into two beams used to excite and to detect the THz pulses with average laser beam powers of 15.1 and 14.8 mW, respectively. As shown in the Fig. 1 inset, the THz pulses were out-coupled vertically by mirror M1 from the confocal THz-TDS system (described in detail in [14] and [15]) and here used as the THz transceiver, placed on the optical table. The vertically reflected THz beam from M1 was directed to the telescope mirror (M3), by the horizontal reflection from mirror M2. The spherical 30.5 cm diameter telescope mirror with a 317.5 cm focal length was placed with the focus at the confocal THz beam waist [14], midway between M1 and M10. The THz collimated beam from M3 was reflected from M4 and M5 and directed to mirror M6 in the Target Building 2, which reflected the beam horizontally to mirror M7 for return to Building 1. Mirrors M6 and M7 form an air-spaced right angle prism (retro-reflector). The returning THz beam was directed to the telescope mirror (M3), by the reflections from mirrors M8 and M4. The center of the returning THz beam on mirror M4 was displaced horizontally, 18 cm from the center of the out-going THz beam on M4. Finally, the focusing reflection of the returning beam by M3 directed the focus to M10, by the vertical reflection from M9. An analysis of the THz beam coupling through a similar long-path indoor system has been presented in [9].

The total round trip path between the transmitter and receiver chips was 185.7 m, which is approximately equal to 52 round-trips of the circulating 50 fs optical pulse within the mode-locked ring laser, thereby, giving sampling pulses delayed by 52 pulses down the pulse train from the excitation pulses. The repetition rate of mode-locked lasers has been shown to be remarkably stable to 6 digits, with some drift and jitter in the 7th and 8th digits [9]. For the indoor system [9], the repetition rate was 89.6948 MHz, and the measured time jitter was less than 0.1 ps. Here, for the outdoor system with clear air and no wind, the jitter is less than 0.1 ps.

In order to measure the coupling loss of the optical train on the optical table, the removable retro-reflector mirrors (M6′ and M7′) were installed inside at the window of the Transceiver Building 1; the outgoing THz beam from mirror M5 was then reflected by M6′ and M7′, as shown in Fig. 1 by the dashed lines. The consequent returning THz beam path from M7′ inside the Transceiver Building 1 was aligned to be on the same path as the returning THz beam from M7. The total round trip

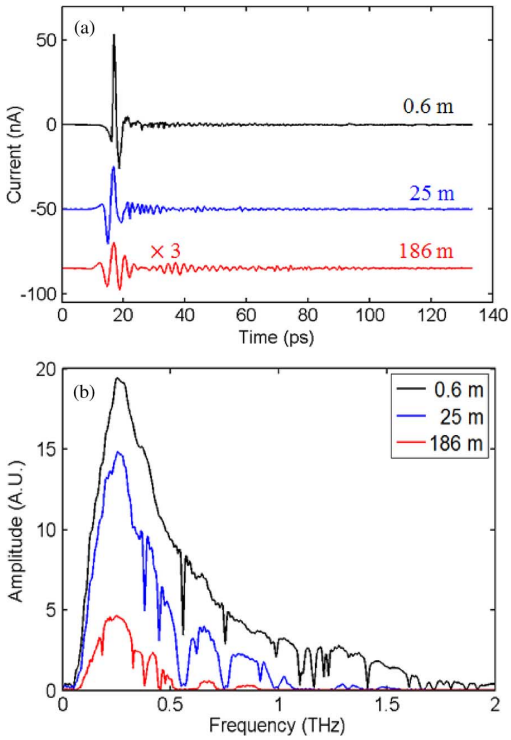

Fig. 2. (a) Measured THz input pulse from 0.6-m long path (upper pulse) and **output pulse** from 25 m path (middle pulse). Measured THz output pulse (lower pulse) with a 3× expanded vertical scale from 186-m long path. (b) Corresponding amplitude spectra for THz input pulse (upper curve), the 25 m output pulse (middle curve) and the 186 m output pulse (lower curve).

path with mirrors M6′ and M7′ in place is 25.0 m, for which the sampling pulses are delayed by 7 pulses down the pulse train from the excitation pulses.

III. Measurements

As shown in Fig. 2, the input and two output THz pulses were measured. Because the upper input THz pulse was measured without mirrors M1 and M10, the total THz beam path from transmitter chip to receiver chip was only 0.6 m. The middle, inside, 25 m short-path THz pulse was measured with the M1 and M10 mirrors and with the M6′ and M7′ mirrors. The outside, 186 m long-path output THz pulse, shown as the lower pulse on a 3× expanded vertical scale. It was measured with M1 and M10 mirrors, without M6′ and M7′ mirrors, and using M6 and M7 mirrors. For the 186-m pulse, the additional oscillations near 40 ps were caused by the combined action of the dispersion and absorption of the water-vapor lines. The RH for the input pulse and the short-path within Building 1 was 45% at 21°C (density 8.4 g/m^3). The RH of the long-path between the buildings was 68% at 16 °C (density 9.2 g/m^3).

The THz pulses are measured by computer controlled mechanical scanning of the relative delay between the detected THz pulse and the optical sampling pulses driving the THz receiver [14], [15]. Here, the THz pulses were measured over a scan duration of 133.2 ps, which corresponded to a frequency resolution of 7.5 GHz. A scan consisted of 1000 data points with 0.1332 ps time steps. This was achieved with 20-μm steps between data points corresponding to a double-pass distance of 40 μm between data points. The total scan has 1000 steps, and a single scan takes 190 s. For sequential measurements over time durations extending to several hours, the data collection runs continuously, whereby the 190 sec. data scan is made, followed by a 30 sec reset, and then the 190 sec. data scan is repeated, and so on.

The corresponding amplitude spectra, obtained by a numerical Fourier transform of the pulses of Fig. 2(a) with zero-padding to a total scan length of 6750 ps, are displayed in Fig. 2(b). Because of much the shorter THz beam path of the input measurement, the input spectrum shows well resolved strong water lines. In contrast, the two output spectra show complete absorption bands for the strong water lines and some weak lines in the low frequency range, which cannot be seen in the input spectrum because of the short beam path.

Because of the relatively short path difference, for frequencies between the water lines and below 1 THz, the spectral amplitude difference between the 0.6 and 25 m beam paths is mainly due to the coupling loss of the complete optical train with mirrors M6′ and M7′ shown in Fig. 1, and not the water vapor absorption. Here, coupling loss is broadly defined to be loss that is independent of the water vapor density. However, the 25-m reduction is not the total coupling loss of the entire optical train with mirrors M6 and M7, because of the additional coupling loss due to the frequency dependent diffraction of the THz beams during the 158.6 m round trip between the two buildings.

For example, consider an out-going, spherical wavefront, 0.25 THz Gaussian beam profile from the collimated transceiver beam waist between M1 and M10 with a 30 cm amplitude ($1/e$) diameter at M3. The reflection from the 30.5 cm diameter telescope mirror M3, with its focus at the transceiver beam waist, collimates the beam with the Rayleigh range of 58.9 m [9], [16]. Because the 25 m short-path is well within the Rayleigh range, the 30 cm amplitude diameter beam remains collimated. However, the returning 186 m long-path Gaussian beam would have a diameter of 95.4 cm at M3 [9], [16]. The corresponding long-path power coupling loss is given by the square of the ratio of the diameter of M3 to the diameter of the incoming beam at M3 (30.5/95.4)=0.320, which is 0.102 [16], equivalent to an additional coupling loss of 9.9 dB. This simple argument would also predict that in Fig. 2(b), neglecting the low water absorption at 0.25 THz, the ratio of the amplitude spectrum of the 186 m path to the 25 m path should be given by the ratio (30.5/95.4)=0.320 in good agreement with the observation.

The transmitted THz pulses and spectra through 186 m with four different RH and temperatures are shown in Fig. 3. Table I shows the corresponding weather conditions outside of the buildings. The RH and temperature inside of the buildings was maintained at 45% and 21 °C (density 8.4 g/m^3) respectively. Because the weather cannot be controlled, the measurement was done on three different days. The THz pulse delays due to the higher RH and water vapor density (WVD) with respect to the first minimum of the top pulse (density 1.1 g/m^3) were 12.8, 23.6, and 37.4 ps as shown in Fig. 3(a).

For Fig. 3(b), if all the experimental parameters remained constant for the different data sets taken over several months, a good THz-TDS measurement of water vapor absorption could be obtained from the ratio of the spectrum of the 11.2 g/m^3 pulse to that of the 1.1 g/m^3 pulse. For this ratio to be accurate, the

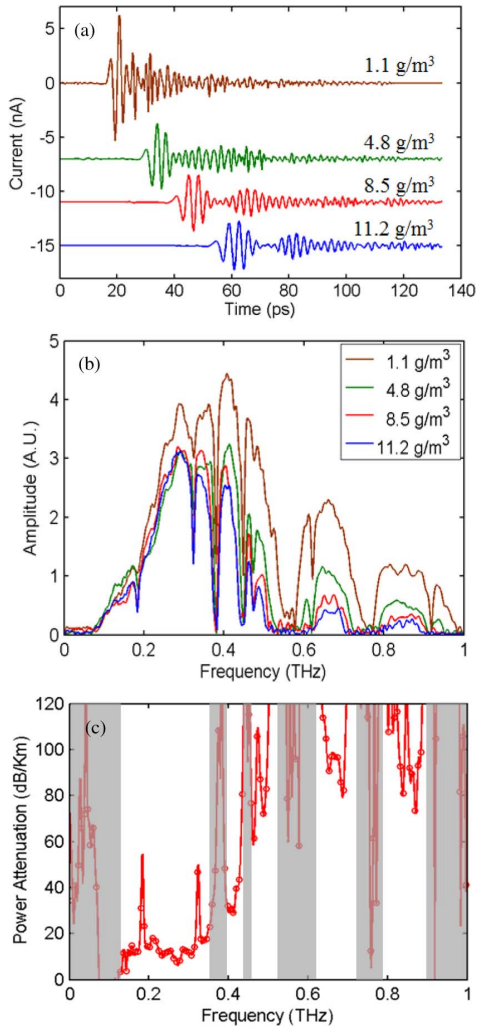

Fig. 3. (a) Measured THz output pulses showing their different transit times for the WVD values of 1.1 g/m^3, 4.8 g/m^3, 8.5 g/m^3, and 11.2 g/m^3. (b) Corresponding amplitude spectra for THz output pulses. (c) Measured power attenuation coefficients in dB/km for the WVD difference of 10.1 g/m^3, between the reference spectrum of 1.1 g/m^3 and sample spectrum of 11.2 g/m^3. The grey regions cover the no-signal areas caused by the strong water vapor absorption lines.

TABLE I
WEATHER CONDITIONS OUTSIDE OF THE BUILDING FOR DIFFERENT RH MEASUREMENTS, SHOWN IN FIG. 3

Measured Date	Relative Humidity (%)	Temperature (°C)	Water vapor Density (g/m^3)	Wind Velocity (m/s)
2014.03.06	12.5	9.6	1.1	1.3
2014.02.25	37.7	14.8	4.8	1.2
2014.04.17	54.0	18.3	8.5	2.9
2014.04.17	73.9	17.6	11.2	3.1

beam coupling ratios and all alignments would need to be the same. Although all of the alignment procedures were the same, there is always small systematic variations, as shown by the out of sequence regions in amplitude spectra comparison, for which the spectral amplitudes should always be in the WVD sequence of 1.1 (highest), 4.8, 8.5, and 11.2 (lowest).

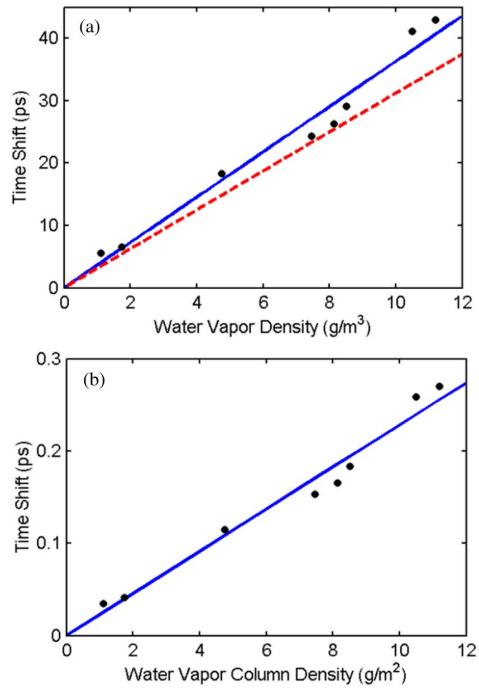

Fig. 4. (a).Measured time shift (dots) for different WVD and fitted line (solid line), for a propagation length of 159 m. The dashed line is from [10], for a propagation length of 137 m. (b) Measurements of (a) re-plotted in terms of column density (g/m)^2. Upper blue line and lower dashed red line of (a) are presented in (b) after division by 159 and 137 m, respectively. They show excellent agreement and overlap.

The corresponding power attenuation shown in Fig. 3(c) is similar in detail to previous work [16], but is approximately 10 dB/km higher from low to high frequencies. For our measurement distance of 159 m, 10 dB/km corresponds to a 20% increase of the input amplitude spectrum for the WVD 1.1 reference pulse, compared to the WVD 11.2 output pulse. These two pulses were measured more than a month apart and such a difference would not be surprising. However, these results demonstrate the feasibility to make informative, long-path, $\pm 1\%$ measurements under various weather conditions.

The time shift of the THz pulses of Fig. 3(a) are shown in Fig. 4(a), as a function of WVD. The dots and solid line indicate the measured time shifts and fitted line, respectively. The data points show the time shifts from the reference pulse vs the difference in WVD, as shown in Fig. 3(a). Therefore, the time shift slope in the figure is determined, by only the WVD outside of the buildings. The slopes of the solid line is 3.63 ps/(g/m^3), while the slope of the dashed line from [10] is 3.12 ps/(g/m^3).

The slope of the solid line is 0.51 ps/(g/m)^3 larger than that of the dashed line because the THz propagation length outside of the building is 22 m longer than the sample chamber length used in [10]. The THz propagation length outside of the building in this measurement is 159 m and the propagation length through the chamber in the [10] is 137 m. The comparative slope is obtained by the following normalization, 3.63 ps/(g/m)^3 $\times$ (137 m/159 m) $=$ 3.13 ps/(g/m)^3, giving excellent agreement between the two values.

This agreement between the two measurements is better expressed by re-plotting the two different measurements in terms

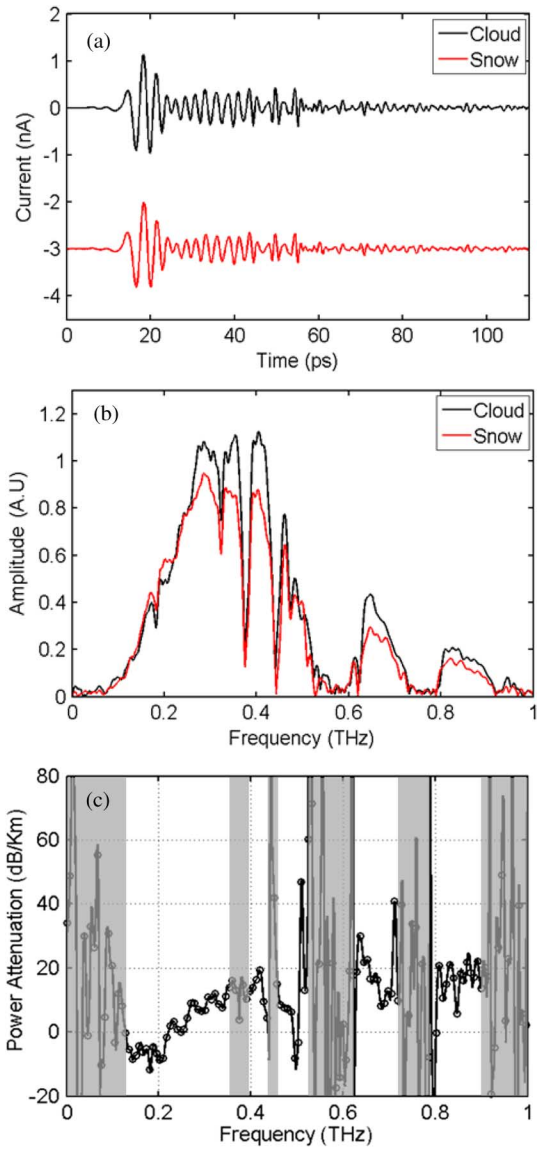

Fig. 5. (a) Measured THz output pulses for the two weather conditions, of cloudy (no snow) upper (black) pulse and cloudy (with snow) lower (red) pulse. (b) Corresponding amplitude spectra for the THz output pulses of (a). (c) Measured power attenuation coefficients in dB/km for the reference spectrum of cloudy (no snow) starting at 100 GHz and the output sample spectrum of cloudy (with snow) shown in Fig. 5(b).

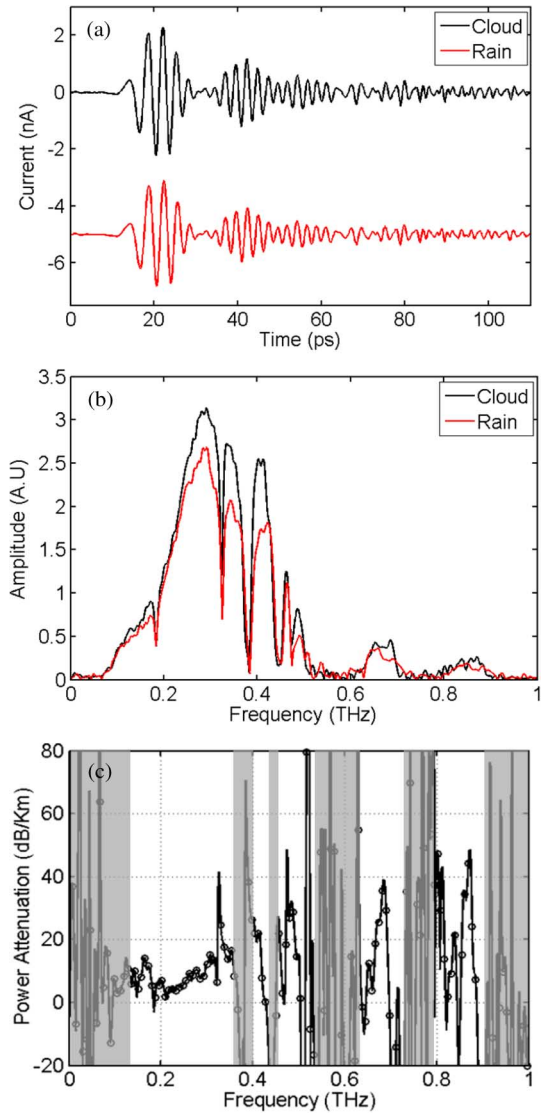

Fig. 6. (a) Measured THz output pulses for the two weather conditions, cloudy (no rain) upper (black) pulse, cloudy (with rain) lower (red) pulse. (b) Corresponding amplitude spectra for the THz output pulses of (a). (c) Measured power attenuation in dB/km for the reference spectrum of cloudy (no rain) starting at 100 GHz and for the output sample spectrum of cloudy (with rain) shown in Fig. 6(b).

of column density $(g/m)^2$, as shown in Fig. 4(b), for which the data points in Fig. 4(a) have been divided by 159 m, and the red dashed line divided by 137 m.

THz-TDS long path studies under the atmospheric weather conditions of clouds, snow and rain can provide important information for THz pulse propagation applications. Here, the first measured THz pulses and corresponding spectra transmitted through snow and rain are shown in Figs. 5 and 6. Table II shows the weather parameters. The amount of snowfall was approximately 2 cm/h which corresponds to 2 mm/h rainfall. The amount of rainfall during the measurement was approximately 3.5 mm/h.

The snow THz pulse measurements and the corresponding amplitude spectra are shown in Fig. 5(a) and 5(b), respectively.

TABLE II
WEATHER CONDITIONS OF CLOUD, RAIN, AND SNOW FOR FIGS. 5 AND 6

Measured Date	Weather	Relative Humidity (%)	Temperature (°C)	Water Vapor Density (g/m^3)	Wind Velocity (m/s)
2014.02.11	Cloud	73.4	4.2	4.5	1.9
2014.02.11	Snow	79.4	2.9	4.4	2.6
2014.04.17	Cloud	73.9	17.6	11.2	3.1
2014.04.17	Rain	88.7	13.8	10.6	1.1

The cloudy (with snow) sample pulses were measured first, and the cloudy (no snow) reference pulse was measured 40 min later. From our operating experience the THz-TDS system stability has been shown to have stable pulseshapes over several hours

with stable weather conditions. Consequently, THz-TDS measurements should be acceptable for this relatively short time period. However, there are relative spectral amplitude fluctuations between the reference and sample spectra in the region of 0.2 THz, for which the snow amplitude exceeds the cloudy amplitude.

The cloudy (with rain) THz pulse measurements and the corresponding amplitude spectra are shown in Fig. 6(a) and 6(b), respectively. The cloudy (no rain) references pulses were measured first, and the cloudy (with rain) sample pulses were measured 5 hours later. The system stability should be acceptable for this time period. Unfortunately, the weather conditions did not allow cloudy reference pulses before and after the snow and rain measurements. The cloud spectrum has higher amplitude than the rain spectrum over the entire range indicating the lack of obvious systematic spectral fluctuations.

The RH, temperatures and corresponding WVD for the reference and sample pulses are given in Table II. The WVD values in Table II are obtained from continuous hygrometer and thermometer measurements of RH and temperature at the single ground station and are assumed to describe the entire 9.5 m elevated long-path between the buildings. In future experiments, it is clearly important to measure RH and temperatures at several positions along the elevated line-of-sight THz beam path between Buildings 1 and 2. This will establish the relationship between the ground and elevated measurements, and define the extent of the variations along the 80 m separation between the buildings.

An important feature of these THz-TDS measurements is their ability to make direct measurements of the WVD$\times$ (path-length) product to establish the consistency of the results. The WVD integrated over the outdoor path can be obtained from the observed minimum amplitude transmission of the weak Handbook 322 GHz water vapor line, for which the calibrated power absorption loss is 46 dB/km at WVD of 10 g/m^3 [16]. For this determination the (no-line) amplitude spectrum without the water line is estimated from Fig. 5(b) and Fig. 6(b). Then the amplitude transmission is obtained from the quotient of the ratio of the minimum spectral amplitude of the 322 GHz line to the no-line spectrum.

From Fig. 5(b) the minimum amplitude transmission of the 322 GHz line is 0.64 for the reference spectrum and 0.65 for the sample spectrum, showing their WVD is almost the same. The sample power transmission $(0.65)^2 = 0.423$, is equivalent to a power loss of 3.74 dB. However, part of this loss is due to the 25 m path in the Transmitter building with RH 45% and 21 $^\circ$C, and WVD $=$ 8.4 g/m^3, giving a power loss of 0.97 dB. Consequently, the power loss due to the 159 m outside path is 2.77 dB, corresponding to a power loss 17.4 dB/km. Given that the calibrated power absorption loss for the Handbook 322 GHz water vapor line is 46 dB/km at WVD of 10 g/m^3 [16], and that loss in dB/km is proportional to WVD, the desired WVD $= (17.4/46)\times 10$ g/m^3 $= 3.8$ g/m^3, which is reasonably consistent with the Table II values of RH and temperature, obtained at the ground station.

For Fig. 6(b), we obtain the minimum amplitude transmission of the 322 GHz line for the cloud pulse and the rain pulse to be 0.40 and 0.30, respectively. Performing the same calculation as in the above paragraph, we obtain WVD $=$ 9.6 g/m^3, for the cloud pulse, and WVD $=$ 13.0 g/m^3 for the rain pulse. The large difference between WVD for the cloud and rain pulses is in disagreement with Table II, and affects our analysis that the increased absorption is due only to the rain.

This difference predicts a pulse delay of the rain pulse compared to the cloud pulse of 12.3 ps, using slope of Fig. 4(a) and the WVD difference. However, this delay was not observed. Either the initial calculation of the line-strengths was imprecise (see below), or the long-path length slightly changed in the 5 hours between the rain data pulses and the reference pulses, or there was an experimental error in the starting time of the reference scans. The convergence between the time delay measurements, the 322 GHz line absorption and the direct measurements of WVD from humidity and temperature is part of our future program to achieve $\pm 1\%$ precision.

The 322 GHz line, minimum transmission method provides an important consistency check, and the logic of the analysis is correct. A feature of a stable data scan is that the weak water lines appear narrow and centered on their Handbook frequencies. Our instrument limited linewidth is 6.5 GHz, and we can determine the line center to ± 1 GHz. If the weather conditions are changing during a measurement scan, the lines are broadened and shifted in frequency. Broadening reduces the apparent line strengths. For small shifts, the measurement should always be of the transmission minimum.

Another, point is that it is difficult to estimate the absorption at line center without water vapor. For an approach to this determination, the amplitude transmission of the 322 GHz line can be calculated, using the van-Vleck Weisskopf lineshape function [17], with the linewidth of 6.5 GHz. The amplitude spectrum is then divided by this transmission. The resulting spectrum will show no evidence of the 322 GHz resonance line, when the WVD-(path-length) product matches the experimental value of WVD. A similar approach has been used to provide a reference spectrum in [18].

As an additional consistency check, the spectrum for the well-defined initial pulse feature of the cloud, snow and rain measurements has been shown to extend from low frequencies up to 0.37 THz [9]. Consequently the amplitude ratios of these features for the snow and rain sample pulses to their cloud reference pulses give averaged measures over this low frequency range of the snow and rain absorption. The measured ratios of 0.88 and 0.82 are evaluated for power attenuation to be 7.1 dB/km for snow and 10.8 dB/km for rain.

In the snow measurement of Fig. 5(c), firstly, we have the unphysical negative absorption up to approximately 200 GHz; this feature is considered to be due to a change in the input spectrum. Then, the measured power absorption of snow in the water line windows shows a monotonically increasing absorption from 200 GHz up to 20 dB/km at 400 GHz, followed by 20 dB/km from 820 to 930 GHz.

In the rain measurement of Fig. 6(c), there is an initial approximately 10 dB/km absorption feature, which we consider to be questionable, and probably due to an input spectral fluctuation. From 200 GHz up to 300 GHz, there is a monotonic increase up to 300 GHz, followed by a loss of sensitivity due to the large difference between the sample WVD and the reference WVD.

The expected attenuation for a rain of 4 mm/h is relatively frequency independent over the frequency range from 0.1 to 1 THz, and has an attenuation of between 3 and 4 dB/km, as shown in [16, Fig. 27]. The rain attenuation curve in dB/km is linearly proportional to the rain rate in mm/hr. A recent single frequency 355 GHz measurement of rain attenuation vs rain rate gave an attenuation of approximately 4 dB/km for 5 mm/h with a great deal of data scatter [19]. As can be seen in Fig. 6(c), the attenuation spectrum shows a both a strong, frequency dependence and a much larger attenuation than are theoretically predicted [16]. This disagreement between theory and experiment will be investigated in future measurements with the goal of $\pm 1\%$ precision.

IV. Measurements With Changing Water

In order to better understand the experimental stability, THz pulses were sequentially measured during changing weather conditions to determine the relationship between time delay and RH variation or wind velocity. Fig. 7(a) and (b) show RH and wind velocity during three sequential measurements. The different background colors indicate each measurement period. Each single scan takes 190 s. The THz pulses were sequentially measured with slowly decreasing RH at 23.8 ± 0.3 °C, from RH 92% (density 20.3 g/m^3) to RH 85%. (density 18.8 g/m^3) and with the approximate wind velocity of 2 m/s. Because the RH and wind velocity are measured on the ground between the two buildings, the values in the THz path have some deviations.

Fig. 7(c) shows the red first and the blue second sequentially measured and over-lapped output pulses. The two pulses do not overlap over the entire scan duration because of the decrease in RH. The second THz pulse leads the first pulse because the RH decreased by approximately 3% over the first scan. The time shift for the first few peaks of the two pulses is shown in the insert of Fig. 7(c).

Fig. 7(d) shows the time shift between two THz pulses. The red, blue, and black measurements and fitting lines indicate the comparisons between the first and second, the second and third, and the first and third, respectively. The dots indicate the measured time shift at every peak and minimum position of the two THz pulses and the solid line indicates the fitted curve to the measured dots. The curves slowly change with an increasing scan time. The time shift between the first and third is larger because there is a 6% change in the relative humidity the two measurements.

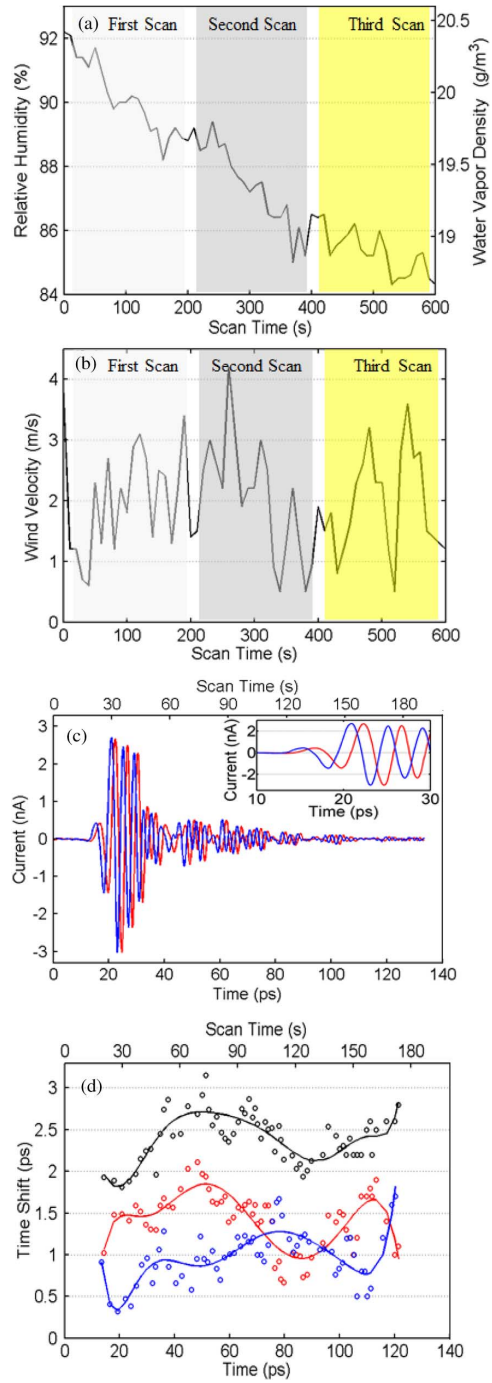

Fig. 7. (a) Measured RH during the first (white), second (grey), and third (yellow) scans. (b) Measured wind velocity during the first (white), second (grey), and third (yellow) scans. (c) The over-lapped, sequentially measured first (red) and second (blue) THz pulses. The insert figure shows the expanded pulses from 10 ps to 30 ps. (d) Measured time shift. The red, blue, and black indicate the comparisons between the first and second, the second and third, and the first and third, respectively. The dots indicate the time shift at each maximum and minimum points of the pulses. The solid line indicates the fitted curve for the dots.

V. Requirements for Precise Measurements

The results presented here are to be considered as a "proof of concept" of the potential of outdoor long-path THz-TDS to characterize the absorption and dispersion of rain and snow in the atmosphere from 100 to 1000 GHz. An important feature is that the measured long-path THz pulses have a signal to noise ratio better than 100 (peak-to-peak of the THz pulse)/(peak to peak of the noise fluctuations in front of the pulse). However, because of experimental constraints and difficulty, the measurements did not have simultaneous reference pulses.

For accurate THz-TDS $\pm 1\%$ measurements the primary experimental problem is to stabilize the system, so that the input pulses remain the same during the measurements of the output pulses. To check that this requirement is satisfied, typically several sequential reference pulses are measured before and after the measurements of the output pulses. For an acceptable stable system, the spectral ratios of the amplitude and phase of sequentially measured pulses must show deviations of less than

$\pm 1\%$ from unity for amplitude and ± 0.05 radians from zero for phase. The driving laser and the beam train are adjusted until this stability is achieved.

The ideal solution would be to simultaneously measure the input pulse and the output pulse, but this has proven to be experimentally difficult. With respect to the Fig. 1 schematic of the setup, this approach would require another THz receiver on the optical table that would be coupled to a non-intrusive beam splitter in the outgoing beam. The beam splitter must not disturb the outgoing beam pattern, must be spatially separated from the incoming return beam, and should not cause any reflections in the time window of the measurement.

Another utilized approach [8]–[11], has the ability to measure the stability of the input THz pulses to the long-path system; for these mirrors M1 and M10 need to be mounted on a 3-ball kinetic base, which can be quickly removed and reinstalled without any changes in alignment. This feature enables the sequential measurement of the stability of the input THz pulses to compare with the above stability criteria. This approach would check the reference pulses before, during, and after the long-path outdoor measurements, which cannot be done with the proof of concept set-up, presented here.

For accurate measurements the sample characteristics need to remain constant during the measurement. This can be monitored by comparison of the measured starting times of sequential output pulses. An acceptable range of the differences would be ± 0.3 ps, corresponding to a change in the water vapor density of 0.08 g/m^3, equivalent to $\pm 0.5\%$ relative humidity at 20 °C. Our measurement gives the integral of the absorption over the long-path, which is simultaneously measured by the weak water lines in the output amplitude spectrum.

Future measurements will also include several simultaneous elevated measurements of RH and temperature along the outside beam path for every data scan. Extensive experimental runs including many sequential reference and sample pulses will be taken under conditions of snow, rain and fog. Data will be analyzed during the run to obtain the best match of WVD for the reference and sample pulses. With such improvements, needed precise $\pm 1\%$ characterizations should be obtained.

VI. Summary and Conclusions

Our proof of concept experiments have shown that THz-TDS long path studies under atmospheric weather conditions have the potential to provide needed $\pm 1\%$ accurate information from 100 to 1000 GHz for THz applications in the atmosphere such as communications and imaging through fog and smoke [12]. The THz output pulses were measured with a signal to noise ratio better than 100, after transmission through a 186 m long round trip path with different RH levels and with the different weather conditions of clouds, rain, and snow. They were compared with reference pulses to determine their attenuation. The measured THz pulse transit time delays were proportional to the water vapor density in agreement with previous indoor measurements with a long-path in a controlled sample chamber. The attenuation measurements were of the order of expectations, but lacked the required $\pm 1\%$ precision due to the lack of simultaneous reference pulse measurements.

References

[1] R. J. Foltynowicz, M. C. Wanke, and M. A. Mangan, "Atmospheric propagation of THz radiation," Sandia National Lab., Sandia Rep. SAND2005-6389, 2005.

[2] R. Blundell *et al.*, "Prospects for terahertz radio astronomy from northern Chile," in *Proc. 13th Int. Symp. on Space THz Tech.*, Cambridge, MA, USA, Mar. 2002, pp. 159–166.

[3] P. Baron *et al.*, "Model for atmospheric terahertz radiation analysis and simulation," *J. Nat. Inst. Inf. Commun. Tech.*, vol. 55, no. 1, pp. 109–121, 2008.

[4] A. Deepak, T. D. Wilkerson, and L. H. Ruhnke, Eds., "Atmospheric water Vapor," in *Proc. Int. Workshop on Atmospheric Water Vapor*, Vail, CO, USA, Sep. 1979, pp. 11–13.

[5] D. E. Burch and D. A. Gryvank, "Continuum absorption by water vapor in the infrared and millimeter regions," in *Proc. Int. Workshop on Atmospheric Water Vapor."*, 1980, pp. 47–76.

[6] R. J. Emery, A. M. Zavody, and H. A. Gebbie, "Measurements of anomalous atmospheric absorption in the range 4 cm^{-1}–17 cm^{-1}," *J. Atmos. Terr. Phys.*, vol. 37, no. 4, pp. 587–594, 1975.

[7] S. Paine, R. Blundell, D. Papa, J. Barrett, and S. Radford, "A Fourier transform spectrometer for measurement of atmospheric transmission at submillimeter wavelengths," *Pub. Astron. Soc. Pac.*, vol. 112, no. 767, pp. 108–118, 2000.

[8] Y. Yang, A. Shutler, and D. Grischkowsky, "Measurement of the transmission of the atmosphere from 0.2 to 2 THz," *Opt. Express*, vol. 19, no. 9, pp. 8830–8838, 2011.

[9] Y. Yang, M. Mandehgar, and D. Grischkowsky, "Broad-band THz pulse transmission through the atmosphere," *IEEE Trans. THz Sci. Technol.*, vol. 1, no. 1, pp. 264–273, Sep. 2011.

[10] Y. Yang, M. Mandehgar, and D. Grischkowsky, "Time domain measurement of the THz refractivity of water vapor," *Opt. Express*, vol. 20, no. 24, pp. 26208–26218, 2012.

[11] Y. Yang, M. Mandehgar, and D. Grischkowsky, "Determination of the water vapor continuum absorption by THz-TDS and molecular response theory," *Opt. Express*, vol. 22, no. 4, pp. 4388–4403, 2014.

[12] Y. Yang, M. Mandehgar, and D. Grischkowsky, "Broadband THz signals propagate through dense fog," *IEEE Photon. Technol. Lett.*, vol. 27, no. 4, pp. 383–386, Feb. 2015.

[13] E.-B. Moon, T.-I. Jeon, and D. Grischkowsky, "Measured THz pulse propagation between buildings," presented at the CLEO-2014, San Jose, CA, USA, Jun. 8–13, 2014, Paper STu1F5.

[14] M. van Exter and D. Grischkowsky, "Characterization of an optoelectronic TeraHz beam system," *IEEE Trans. Microw. Theory Techn.*, vol. 38, no. 11, pp. 1684–1691, Nov. 1990.

[15] G. Gallot, S. Jamison, R. W. McGowan, and D. Grischkowsky, "THz waveguides," *J. Opt. Soc. Amer. B.*, vol. 17, pp. 851–863, 2000.

[16] Y. Yang, M. Mandehgar, and D. Grischkowsky, "THz-TDS characterization of the digital communication channels of the atmosphere and the enabled applications," *J. Infrared, Millim. THz Waves*, pp. 1–33, 2014.

[17] Y. Yang, M. Mandehgar, and D. Grischkowsky, "Understanding THz pulse propagation in the atmosphere," *IEEE Trans. THz Sci. Technol.*, vol. 2, no. 4, pp. 406–415, Jul. 2012.

[18] M. Mandehgar, Y. Yang, and D. Grischkowsky, "Experimental confirmation and physical understanding of ultra-high bit rate impulse radio in the THz digital communication channels of the atmosphere," *J. Opt. Inst. Phys.*, vol. 16, no. 094004, p. 17, 2014.

[19] S. Ishii, S. Sayama, and T. Kamei, "Measurement of rain attenuation in terahertz wave range," *Wireless Eng. Technol.*, vol. 2, pp. 119–124, 2011.

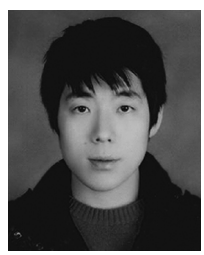

Eom-Bae Moon received the B.S. and M.S. degrees in electrical and electronics engineering from the Korea Maritime and Ocean University, Busan Korea, in 2013 and 2015, respectively.

Tae-In Jeon received the B.S. and M.S. degrees in physics and electronics from Dong-A University, Busan Korea, in 1988 and 1990, respectively, and the Ph.D. degree in the School of Electrical and Computer Engineering, Oklahoma State University, Stillwater, OK, USA, in 1997, under the guidance of Prof. D. Grischkowsky. His Ph.D. dissertation was on the terahertz time-domain spectroscopy of semiconductors.

In 1998, he joined the Division of Electrical and Electronics Engineering, Korea Maritime and Ocean University, Busan, Korea, as an Assistant Professor, and was subsequently promoted to Associate Professor and Full Professor. In the early years of his research, he focused on the characterization of the electrical and optical properties of carbon nanotubes and conducting polymers. After visiting professor at Oklahoma State University from 2004 to 2005, terahertz waveguides have been added to his interests.

Daniel R. Grischkowsky (SM'90–F'92) received the B.S. degree from Oregon State University, Corvallis, OR, USA, in 1962, and the Ph.D. degree from Columbia University, New York, NY, USA, in 1968.

In 1969, he joined the IBM Watson Research Center, Yorktown Heights, NY, USA. In 1993, he joined Oklahoma State University, Stillwater, OK, USA, where his work has concentrated on unique applications of THz-TDS, including waveguides, the Sommerfeld wave, sur-face waves, hole arrays and photonic crystals.

Dr. Grischkowsky is a Fellow of the Optical Society of America (OSA), and the American Physical Society. He was awarded the 1985 Boris Pregel Award by the NY Academy of Sciences, the OSA 1989 R. W. Wood Prize, the OSA 2003 William F. Meggers Award, and the 2011 Kenneth J. Button Prize from the International Society of IR, MM and THz wave.